

Two-Agent Formation Control of Magnetic Microrobots in Two Dimensions

Mohammad Salehizadeh · Eric Diller

Received: date / Accepted: date

Abstract This paper presents a new method to control multiple micro-scale magnetic agents operating in close proximity to each other for applications in microrobotics. Controlling multiple magnetic microrobots close to each other is difficult due to magnetic interactions between the agents, and here we seek to control those interactions for the creation of desired multi-agent formations. We use the fact that all magnetic agents orient to the global input magnetic field to modulate the local attraction-repulsion forces between nearby agents. Here we study these controlled interaction magnetic forces for two cases: i) agents with free 3D magnetization, and ii) agents with constrained magnetization to horizontal motion plane. Accordingly, we devise two controllers to regulate the inter-agent spacing, heading and position of the set, for motion in two dimensions. Simulation and experimental demonstrations on two agents in this paper show the feasibility of the idea and its potential for the completion of complex tasks using teams of microrobots. Average tracking error of less than $39 \mu\text{m}$ and 1.45° is accomplished for the regulation of the inter-agent space and the pair heading angle, respectively, for identical spherical-shape agents with nominal radius less than of $250 \mu\text{m}$ operating within several body-lengths of each other.

Keywords Microrobot · Multi-agent control · Underactuated system · Magnetic actuation · Motion planning

1 Introduction

Microrobots can effectively access small remote spaces with a wide range of potential applications in drug delivery [1],

Eric Diller
E-mail: ediller@mie.utoronto.ca
Mohammad Salehizadeh
E-mail: msalehi@mie.utoronto.ca

Department of Mechanical and Industrial Engineering
University of Toronto, Toronto, Ontario M5S 3G8, Canada

cell lysis/sorting [2], micro-assembly/disassembly [3], and distributed sensor networks [4]. The ability to exert independent control over a team of microrobots working together on a task has potential to increase task speed and capability [5]. Among many proposed strategies [6], remote actuation using a magnetic field is a common choice because it can penetrate most materials, remotely generate both forces and torques on magnetic materials, and is easy and safe to generate and manipulate [7, 8]. However, swarm control of magnetic micro-agents remains an open-ended problem as in most actuation systems, all magnetic micro-agents share a global driving magnetic signal. In this way, all agents receive identical control inputs and thus it is difficult to steer independently for complex task completion [9, 10]. Outside the microrobotics field, several approaches to particle assembly have been explored. For instance, fluidic interactions are considered to achieve dynamic self-assembly of magnetized objects such as magnetic disks [11], gears [12], and colloidal asters [13]. These particles rotate at a liquid-air interface with complex behaviors and motions that are not possible with conventional systems, but are limited to two-dimensional applications. In the microrobotics field, a variety of approaches have been explored: Martel et al. [14] achieved swarm control of bacterial actuators in the human microvasculature trackable by a clinical MRI system. Diller et al. [10] employed geometrically or magnetically distinct microrobots to realize independent control of small teams of magnetic agents. Cappelleri et al. [15] utilized row-column planar addressing micro-coils made with printed circuit board (PCB) technology to localize the field driving magnetic robots. Becker et al. [16] exploited differences in cell population to steer cells to goal positions using ensemble control. Mellal et al. [17] incorporated optimal linear quadratic integrator (LQI) control to navigate two magnetic microbeads independently in 1D. Nevertheless, all these studies have been done only for a small number of agents or entangled with severe limitations such as a lack of path-following capability.

These studies on magnetic micro-agents are also limited

in how close the agents can operate to one another. When they do operate close together, the agents exert large magnetic interaction forces on one another, which results in control instability. Such interactions have been used to attach nearby magnet micro-agents together [18], but have not allowed for independent agent operation in close proximity without coming into contact. Most work in the field of magnetic micro-agents assume that inter-agent magnetic fields are small in comparison with the driving actuation field strength, with the associated requirement that the agents be kept far apart from each other (typically several microrobot body-lengths). This constraint limits the ability of teams of agents from working close together. In Miyashita et al. [19], local magnetic interaction forces are used to create a few stable formations in two dimensions of a set. These formations are modulated by dynamically remagnetizing some of the agents, with promise for controlling sets of up to three agents and limited control over a four-agent set. However, that method is limited to a small set of stable configurations, has no control over the formation orientation, cannot be generalized to microrobots moving in three dimensions, and is only applicable to sets of agents which are each magnetically unique (and so cannot scale up to larger sets of agents).

Here we pursue a more general approach for the dynamic regulation of the inter-agent magnetic forces between nearby microrobots. We model the radial and transverse magnetic forces between these agents, and devise a set of controllers to maintain any desired inter-agent separation, pair heading and center of mass position, in the presence of these forces. In [20], we introduced our preliminary results for the stable motion control of two identical disk-shape magnetic microrobot agents operating in close proximity with the magnetization constrained to the horizontal motion plane. This study now considers the agents' motion in two dimensions with spherical shape while we allow the agents to rotate out of plane as well as in plane. We compare our previous method in [20] for the constrained magnetization with our new method for the free 3D magnetization. To this end, the spatially-uniform external field creates only torque to orient micro-agents and as a result the inter-agent force appears between agents. We modulate the agents' magnetic moment angles to regulate this force. Previous studies have investigated the inter-agent spaces larger than 30 of the agent body radius (R), so that the local forces can be neglected, without loss of generality. Our close proximity region of interest covers the agents pairwise separations between 2.5 to $30R$. Using larger applied fields and faster controllers this range can be extended.

The underlying work enables the full 2D motion control of the two-agent configuration. Controlling larger number of agents will experience even stronger underactuation. This problem will require applying more advanced controllers, including fitness function optimization, robust adaptive control, and stochastic control.

The paper is structured as follows. Section 2 describes the kinematics of agents along with the inter-agent force

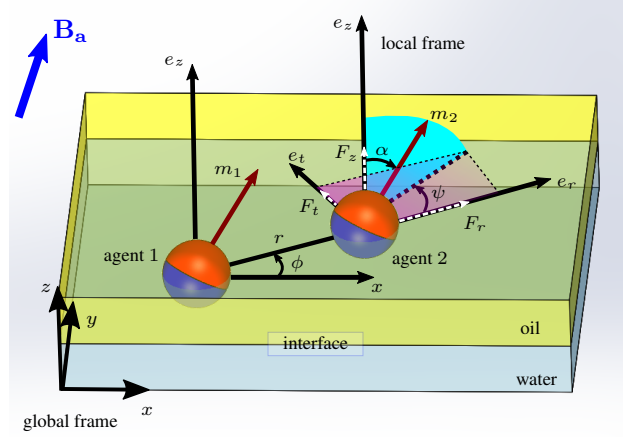


Fig. 1 3D pairwise orientation parameters defined in global and local coordinates for agents in close proximity with magnetic moments m_1 and m_2 aligned with the actuation field B_a . The pairwise distance vector connecting agent 2 to agent 1, and the pair orientation are denoted by r and ϕ , respectively. The radial and transverse coordinates are shown by e_r and e_t . The 2D motion of the agents occurs at the interface between water and oil. The out-of-plane angle that magnetization M makes with the z -axis within the cyan plane is denoted by α and the in-plane angle that the projection of magnetization makes with the radial axis in the motion plane (in purple) is shown by ψ . The radial, transverse, and out-of-plane forces are represented by F_r , F_t , and F_z , respectively, exerted on the second agent by the first agent (corresponding forces acting on agent 1 are not shown).

relation. Section 3 introduces our control principles to regulate the relative motion of agents; accordingly, a systematic feedback control law is synthesized to handle best performance. In section 4, a simulation based on a physical model is conducted to enable prediction of agents behaviors; afterwards, fabrication method and experimental setup that is used to control the relative position of agents are presented, then experimental results are carried out. This paper is concluded in section 5.

2 Concepts and Definitions

This section introduces the kinematics describing a pair of agents along with the inter-agent force relation, and lays the foundation for controlling a two-agent configuration.

2.1 Magnetic actuation and inter-agent kinematics

Following the convention, magnetic flux density is denoted by B . A magnetic moment m represents the field orientation of a magnetic microrobot agent. Under the act of an external magnetic field or via local magnetic interaction with other agents of a set, each agent may experience both force F_m and torque τ , which can be calculated by $F_m = (m \cdot \nabla)B$ and $\tau = m \times B$, where ∇ here is the material gradient [21]. We base our analysis on the assumption that the magnetic moment m of all magnetic agents in the workspace align with the applied field B_a . We use the angle(s) of the applied field as our control input(s) to the entire system. Consider

two identical magnetic agents with magnetic moments \mathbf{m} aligned with the uniform external magnetic field \mathbf{B}_a applied in the workspace for actuation in a two-dimensional (2D) horizontal plane. As the applied field is uniform over space, no external magnetic forces are generated ($\nabla \mathbf{B}_a = 0$). In local Cartesian coordinates ($\hat{e}_r, \hat{e}_t, \hat{e}_z$), the radial, transverse, and normal components of the local magnetic force exerted on the second agent by the first agent can be written as

$$F_r = \frac{\Omega}{r^4} [1 - 3 \sin(\alpha)^2 \cos(\psi)^2], \quad (1a)$$

$$F_t = \frac{\Omega}{r^4} [\sin(\alpha)^2 \sin(2\psi)], \quad \text{and} \quad (1b)$$

$$F_z = \frac{\Omega}{r^4} [\sin(2\alpha) \cos(\psi)]. \quad (1c)$$

Here $\Omega := \frac{3\mu_0 m_1 m_2}{4\pi}$ is the force constant. μ_0 is the permeability of free space, ψ is the local in-plane control input angle defined as the angle between the projection of the actuation field \mathbf{B}_a and the vector \mathbf{r} in the motion plane as sketched in Fig. 1. Similarly, $\psi_G = \psi + \phi$ is the in-plane control angle in global coordinates. α is the out-of-plane (tilting) control input angle measured down from the z -axis. Depending on the magnetization's degrees of freedom (DOF), two scenarios can be discussed as follows:

2.1.1 Free 3D magnetization (2 DOF)

This part explains the case where the agents are capable to magnetically rotate in 3D. In other words, both out-of-plane and in-plane rotations are feasible. To realize this assumption, we use spherical agents with minimal surface area to demand least agent-liquid surface energy. As such, magnetization orientation can be characterized freely in 3D by 2 DOF variables ψ and α .

2.1.2 Magnetization constrained to horizontal plane (1 DOF)

We designated this scenario in [20] for disk-shape agents, where it is assumed that agents are not capable to magnetically rotate out of plane, as the strong surface tension between agent and liquid dominates over the magnetic force. Hence, we constrain the magnetic field to lie in the horizontal plane along the liquid surface and establish our controller. Consequently, agents will rotate in 2D only. As such, magnetization orientation can be characterized by 1 DOF variable ψ . One can consider this scenario as a special case of the first one by putting $\alpha = 90^\circ$.

These force components as a function of control angle ψ are sketched in Fig. 2. From this figure, we can see how to develop a controller for the modulation of the inter-agent magnetic force as a function of the control angle ψ only. At $\psi = 0^\circ$ and $\psi = \pm 90^\circ$ the radial force attains its maximum attractive (negative) and repulsive (positive) value, respectively. It is to be noted that the magnitude of the attractive force is roughly twice as large as that of

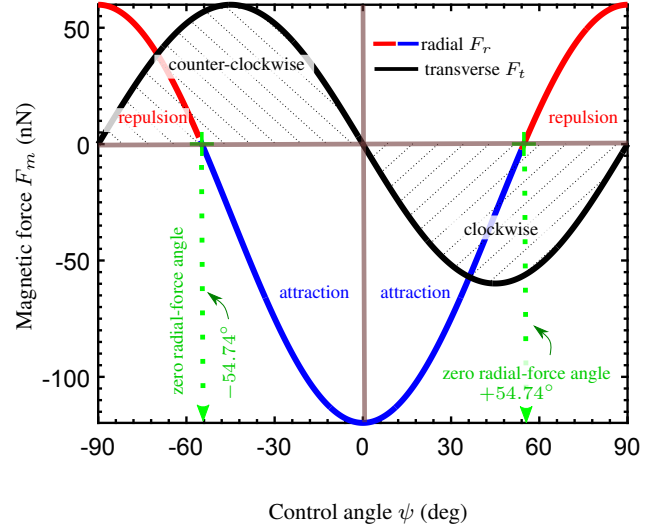


Fig. 2 Inter-agent magnetic force versus control angle based on eq. (1), for the case of $r = 5R$ (R denotes the radius of agents), $|M| = 10^4$ A/m, and $\alpha = 90^\circ$. The critical angles here include: $\psi = 54.74^\circ$ corresponding to the zero-radial force angle, $\psi = 0^\circ$ and $\psi = \pm 90^\circ$ at which the radial force becomes maximum attractive (negative) and repulsive (positive) value, respectively.

the repulsive force. Importantly, at $\psi = 54.74^\circ$ the radial force becomes zero. Also, at any angle between 0 and 90° , a non-zero transverse force occurs which causes the pair of agents to rotate about one another. The transverse force peaks at 45° . Additionally, it can be seen from the figure that the radial and transverse forces are even and odd functions of the control angle about 0° , respectively. In other words, by reflecting the control angle about $\psi = 0^\circ$, the transverse force can be reversed without affecting the radial force. This reflection will be used to control the pair heading ϕ .

2.2 Magnetic field strength requirement

The total field at the location of agent (i) is the vector sum of the inter-agent field \mathbf{B}_{ij} (field on agent i created by agent j) and the actuation field \mathbf{B}_a . It is convenient to assume that the global field \mathbf{B}_a dominates the local field such that all agents always align with the actuation field. Here we check our assumption that the local field created by a nearby agent does not rotate the total field at an agent's location. To avoid this phenomenon, the actuation field strength can be chosen to keep the total field angle error less than a threshold given by $\theta_\varepsilon = \gamma_a - \gamma$, where γ_a and γ respectively represent the actual and desired direct angles made between the total field and external field with the radial coordinate r . One can express the desired angle γ as a function of in-plane ψ and out-of-plane α angles with $\gamma = \cos^{-1} \left[\frac{\sin(\alpha)(1 + \cos(2\psi))}{2 \cos(\psi)} \right]$. Also, the actual angle associated to the total field can be calculated as $\gamma_a = \angle \mathbf{B}_{tot} = \angle (\mathbf{B}_a + \mathbf{B}_{ij})$. For a given angle error threshold θ_ε , the minimum required field strength B_{min} in this case is

$$B_{min} = \frac{b - \sqrt{b^2 - 4ac}}{2a}. \quad (2)$$

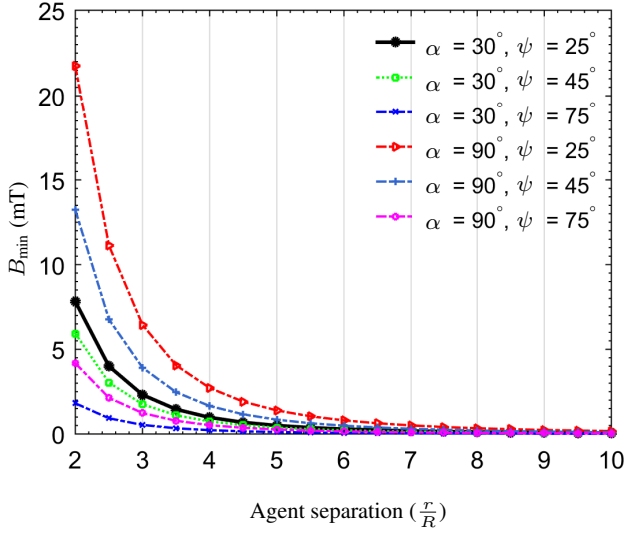


Fig. 3 Minimum required input field strength as a function of agent separation r for multiple control angles α and ψ to limit the total angle error to $\theta_\varepsilon = 5^\circ$ ($|M| = 10^4$ A/m). R denotes the radius of agents.

Where

$$a = \frac{1}{A_1^2} - \frac{1}{A_2^2}, \quad (3a)$$

$$b = \frac{\mu_0 m \left(\frac{4}{A_1^2} + \frac{2}{A_2^2} - 3 \right)}{4\pi r^3}, \quad (3b)$$

$$c = \frac{-\mu_0^2 m^2 \left(\frac{-4}{A_1^2} + \frac{1}{A_2^2} + 6 \right)}{16\pi^2 r^6}, \quad (3c)$$

where $A_1 = \cos(\theta_\varepsilon + \cos^{-1}(A_2))$, and $A_2 = \cos(\psi) \sin(\alpha)$.

Fig. 3 illustrates the minimum required field strength for both 1-DOF case with $\alpha = 90^\circ$ and 2-DOF case with free 3D magnetization as a function of agent separation r for multiple control angle inputs, using a maximum angle error of $\theta_\varepsilon = 5^\circ$. For the experimental section of this paper, agent spacing is roughly $4R$, so we maintain a field strength of 10 mT to be higher than the minimum required and assume that the agents always align with B_a .

2.3 Other forces

2.3.1 Fluid drag force

The microrobots used in this study are spheres with the nominal radius of $250 \mu\text{m}$, and are experiencing low Reynolds number laminar fluid flow with a negligible net acceleration (inertia) on each agent. Therefore, a first-order model is considered to describe the agents motion based on the Stokes fluid drag model as

$$\dot{\mathbf{x}} = -\frac{\mathbf{F}_m}{\sigma}, \quad (4)$$

where $\dot{\mathbf{x}}$ is the induced agent velocity and \mathbf{F}_m is the inter-agent magnetic force. The term $\sigma = 6\pi\mu R$, fluid drag constant, depends on liquid viscosity, μ , and the radius of the spherical agents, R .

2.3.2 Capillary force

In this work, we restrict the agents to operate at water-oil interface. As a special case, having agents immersed at water-oil interface will enable us later to easily extend our model for 3D motion. The agents stay suspended at the interface by capillary forces. Depending on the materials used for the agents and the liquid container, horizontal capillary forces between agents and between the container and the agents may exist [11]. Our estimation shows these forces have a magnitude 100 times less than the magnetic force; in other words, the observation meets our assumption that the capillary force impact is negligible against the magnetic force at the operating separation range for a water-oil interface.

3 Control of Two-Agent Configuration

This section presents our approach to regulate the agent separation r and pair heading angle ϕ . The task in designing a controller is to choose the input magnetic field angle(s) to push the relative spacing and pair heading angle toward the goal state.

3.1 One-input control (ψ)

The purpose of this part is to design a controller for the constrained scenario introduced in 2.1.2, whereby magnetization is constrained to horizontal plane. Therefore, there is only the in-plane rotational angle ψ available as the single global control input and the system is underactuated. The basis for producing the associated radial and transverse forces is shown in Fig. 4(a). We start with the simplest radial controller with two input states, then generalize to a proportional radial controller. Finally we introduce a transverse angle controller well-suited for the constrained mode.

3.1.1 Radial (separation r) control

The simplest radial controller has two states as illustrated in Fig. 4(a) (i-ii). These two states lead to repulsion or attraction of the two agents, when their moments are perpendicular or parallel to their separation vector, respectively.

- (i) If the space between two agents is too small ($r < r_{\text{des}}$), the controller points the field orientation perpendicular to their separation vector \mathbf{r} so that the agents repel each other with full radial force. This is done by applying $\psi = 90^\circ$. The transverse force at $\psi = 90^\circ$ is zero.
- (ii) If the space between two agents is too large ($r > r_{\text{des}}$), the controller points the field orientation parallel to their separation vector \mathbf{r} so that the agents attract each other with full radial force. This is done by applying $\psi = 0^\circ$. The transverse force at $\psi = 0^\circ$ is zero.

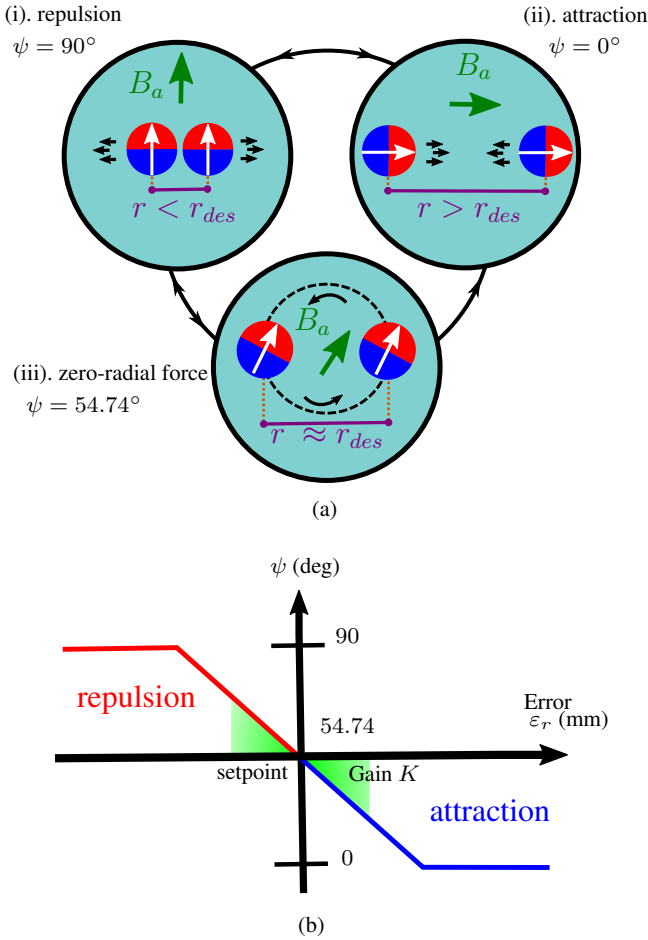


Fig. 4 Two-agent configuration control principle. (a) States of agent attraction or repulsion are determined by the direction of applied field B_a : i) repulsion at $\psi = 90^\circ$, ii) attraction at $\psi = 0^\circ$, iii) zero radial-force at $\psi = 54.74^\circ$. (b) Radial proportional controller design.

(iii) (optional) If the space between two agents is close to the goal spacing ($r \approx r_{des}$), the control angle is set to $\psi = 54.74^\circ$ such that the radial force is zero. In this state, a transverse force is created which rotates the pair (we ignore this rotation for now).

To enhance the level of precision, a more sophisticated controller would choose intermediate angles between those shown in Fig. 4(b), centered around the zero-radial force angle. To create a proportional controller (P-controller), we define the radial separation error $\varepsilon_r = r - r_{des}$, which allows us to give the proportional control law as $\psi = \psi_s - K\|\varepsilon_r\|$. Thus, the controller applies a larger radial force correction for larger separation errors ε_r (up to saturation) as shown in Fig. 4(b). The gain K is tuned manually to result in a stable controller with good performance.

3.1.2 Angle (pair heading ϕ) control

For control angle inputs between $\psi = 0^\circ$ and 90° , a transverse force F_t will be induced on the agents according to eq. (1b). If we wish to control the pair heading ϕ , we can choose the sign of this transverse force by choosing

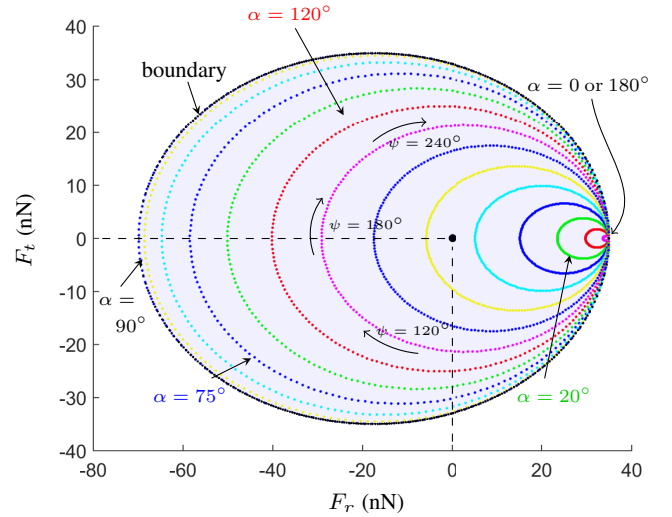


Fig. 5 Bounds of achievable forces as control inputs ψ and α sweep. ψ and α vary from 0 to 360° and from 0 to 180° , respectively. Having two control inputs we are able to create motion that spans the entire space within the boundary leading to full actuation.

whether we operate with positive or negative values of ψ as shown in Fig. 2. Because F_r is symmetric about $\psi = 0^\circ$, reversing the sign of ψ does not affect the radial controller already introduced. Although we cannot arbitrarily choose desired values of both F_r and F_t , we can regulate the radial force proportionally while introducing a bang-bang type binary controller on the transverse force. We choose to keep the proportional controller on the radial rather than the transverse force because this coordinate tends to be unstable (due to the r^{-4} relationship on F_r in eq. (1a)). For more information, see section 1 in the supplementary material [S1] for a discussion on the coupling behavior of the states. Using this scheme, the control of the two parameters r and ϕ can be regulated using a single magnetic global input. In the next section, the effectiveness of this control method is characterized.

3.2 Two-input control (ψ and α)

Here we aim to design a new controller for the general scenario discussed in 2.1.1 on the freely rotating 3D magnetization. In particular, the system with two states of separation r and pair heading angle ϕ can now be fully actuated having two control input angles, ψ and α . Fig. 5 demonstrates bounds of achievable forces F_r and F_t in the plane of motion that agents exert on one another, as the control inputs ψ and α sweep. This figure indicates that with two inputs we are able to create motion that spans the entire space leading to full actuation. Without loss of generality, we make this assumption that magnetic tilting force F_z will be counteracted by the surface tension at the liquid interface. Thus, using this new controller the spherical agents still swim in the 2D plane while they align with the applied field in 3D due to their feasible free rotation.

3.2.1 Straight line motion error definition

Another key advantage of the two-input control method over the one-input control is that back to its full-actuation property, the new controller lends itself to steer agents in the shortest path along a straight line toward the goal state. The error can be calculated as

$$\varepsilon_r = 0.5 [r - r_{\text{des}} \cos(\Delta\phi)], \text{ and} \quad (5a)$$

$$\varepsilon_t = 0.5 r_{\text{des}} \sin(\Delta\phi). \quad (5b)$$

Here r and r_{des} represent the actual and desired separations, respectively. The pair heading angle ϕ error is denoted by $\Delta\phi$. The radial and transverse errors are represented by ε_r and ε_t , respectively. For more information on how to derive the above equations, see section 4 in the supplementary material [S1].

3.2.2 Control law

The control policy is to apply force in the opposite direction of error. One can calculate desired forces ${}^{\text{des}}F_r$ and ${}^{\text{des}}F_t$ from the radial and transverse error vector $\varepsilon = [\varepsilon_r \ \varepsilon_t]^T = -K \left[\frac{{}^{\text{des}}F_r}{\sigma} \ \frac{{}^{\text{des}}F_t}{\sigma} \right]^T$ and then find the control inputs ψ and α from eq. (6) taking into account the given boundary inequality. Here K is the regulator gain to tune the forces.

$$\tan(\psi) = \frac{3}{2} \frac{r^4 F_t}{\Omega - r^4 F_r}, \quad (6a)$$

$$\tan(\alpha) = \sqrt{\frac{-4r^8 F_r^2 - 8r^4 F_r \Omega + 9r^8 F_t^2 + 4\Omega^2}{4r^8 F_r^2 + 4r^4 F_r \Omega + 9r^8 F_t^2 - 8\Omega^2}}, \quad (6b)$$

$$\text{subject to} \quad -2\frac{\Omega}{r^4} \leq F_r \leq \frac{\Omega}{r^4} \text{ and} \\ |F_t| \leq \frac{2}{3r^4} \sqrt{-r^8 F_r^2 + 2\Omega^2 - \Omega r^4 F_r}, \text{ where } \Omega > 0$$

4 Results

This section presents numerical simulation results, the fabrication process and experimental setups, and the experimental results of the proposed control techniques for two-agent configuration.

4.1 Simulations

A simulation environment based on the proposed physical model is designed to enable prediction of agents behaviors under the act of controller so as to be able to justify and optimize the experimental observations. Afterwards, by doing experiment we can validate and update the simulation outcomes.

4.1.1 One-input control simulation

Fig. 6 shows numerical simulation of the motion trajectory of magnetic agents in two-agent configuration using the one-input controller. This simulation is a time integration of eq. (1) for initial condition of $r = 3.5R$ and parameters

$|M| = 10^4$ A/m, $\mu = 8.9 \times 10^{-4}$ Pa.s. Since the agents have a spherical shape, it is admissible to use the fluid drag force eq. (4). The agent-to-agent capillary force and agent-liquid-wall capillary force, as well as inertial forces are ignored in the simulation. The simulation shows a particular case in repulsion mode where two agents are initially too close ($r = 3.5R$). The desired pairwise separation r_{des} is reached when the sketched surrounding dashed-line circles around agents with radius equal to $0.5r_{\text{des}}$ come into contact with one another. Initial positions are denoted by circle and current positions with diamond. Here the agent radius is $250 \mu\text{m}$. The desired separation and pair heading are set at $7R$ and 45° , respectively. It can be seen that the controller approaches the goal configuration and the error reduces to a small value over time. We have seen in simulation that the controllers are stable for a wide variety of initial conditions. The switching behavior of the control input is apparent both in the trajectory inset and in the time-series graph in Fig. 6.

4.1.2 Two-input control simulation

Fig. 7 shows numerical simulation of the motion trajectory of magnetic agents in two-agent configuration using the two-input controller, constructed in a similar way as the previous part. One important distinction of this new controller is that it lends itself to steer agents in the shortest path along a straight line toward the goal state, whereas using one-input control method the two states are coupled to each other. It can be seen that the controller approaches the goal configuration and theoretically the error reduces to zero over time.

4.2 Fabrication of agents and experimental setup

4.2.1 Spherical agents

Our identical spherical agents are composed of either polyurethane polymer (BJB M-3184) or as an alternative a stiff silicone elastomer material (Sylgard 184, Dow Corning), which is mixed homogeneously with permanent magnetic particles (MQFP-15-7, NdPrFeB, Magnequench) at a mass ratio of 2:1, combined with hollow glass beads (3MTM Glass Bubbles K20) at a mass ratio of 10:1 to make the agents neutrally buoyant in order to float at the interface. These smooth spheres can be produced in a batch process using a fluid-assisted method as shown in Fig. 8. We describe briefly this fabrication process involving: (1) Degas the prepared uncured composite in a vacuum pump. (2) Use a needle to inject this soft composite into a high viscous fluid such as 1000 cSt (25°C) silicone oil, honey, or corn syrup inside a beaker followed by a needle swirl. Afterwards, spheres are formed perfectly due to capillary force condensation. (3) Cure for 12 hours. (4) Clean the spheres using water.

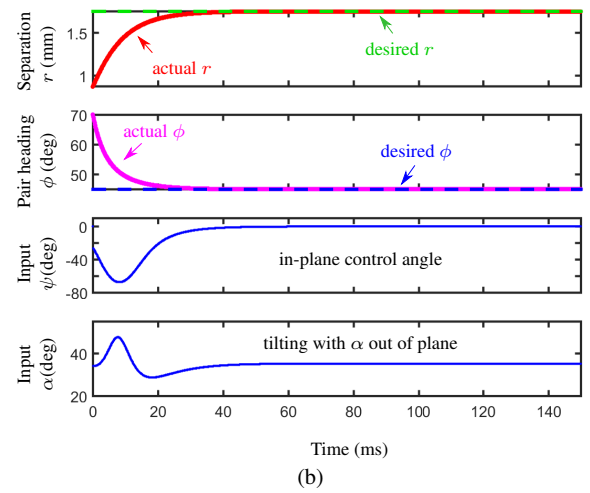
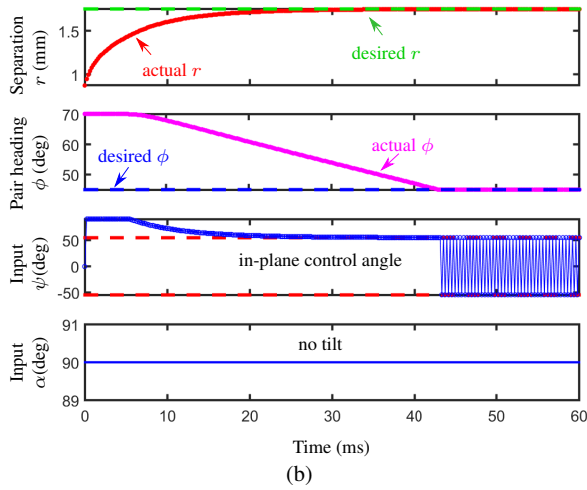
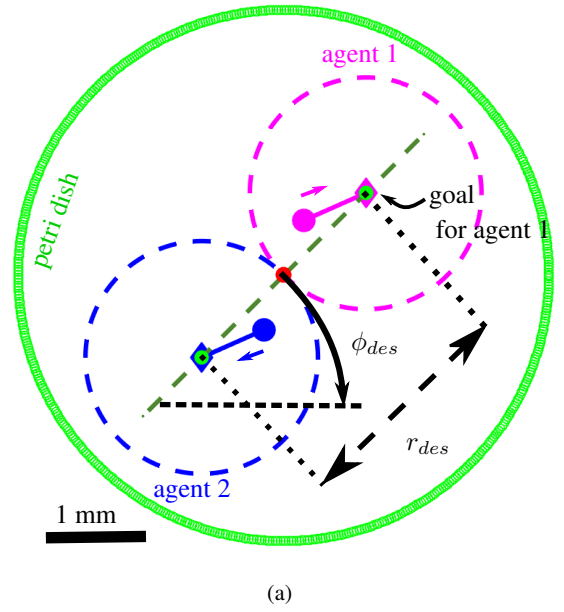
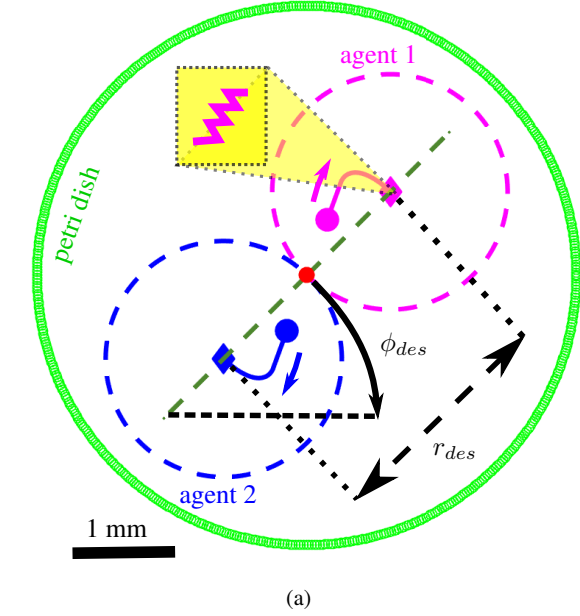


Fig. 6 Two-agent configuration control simulation using one-input control method. (a) Motion trajectory in repulsion mode. (b) Time evolution of separation r and pair heading angle ϕ states along with the control input ψ . The top plot shows the motion trajectory simulation in solid line. The desired pairwise separation r_{des} is reached when the sketched surrounding dashed-line circles around agents with radius equal to $0.5r_{des}$ come into contact with one another. Initial positions are denoted by circle and current positions with diamond. Here the agent radius is $250 \mu\text{m}$, the initial separation is $r = 3.5R$ assuming the desired separation and pair heading are set at $7R$ and 45° , respectively, and $|M| = 10^4 \text{ A/m}$. The trajectory inset shows how controller switches the input sign to maintain the pair heading angle at the goal.

4.2.2 Experimental setup

Magnetic fields for agent actuation are created in an electromagnetic coil system with three pairs of coils nested orthogonally to create fields in 3D, powered by three pairs of analog servo drives (30A8, Advanced Motion Controls). Each pair of wire loops in the coil system is arranged in Helmholtz configuration, resulting in a uniform magnetic field up to 15 mT (uniform to within 5% of nominal at the

Fig. 7 Two-agent configuration control simulation using two-input control method. (a) Motion trajectory in repulsion mode. (b) Time evolution of separation r and pair heading angle ϕ states along with the control inputs ψ and α . The top plot shows the motion trajectory simulation in solid line. The desired pairwise separation r_{des} is reached when the sketched surrounding dashed-line circles around agents with radius equal to $0.5r_{des}$ come into contact with one another. Initial positions are denoted by circle and current positions with diamond. Here the agent radius is $250 \mu\text{m}$, the initial separation is $r = 3.5R$ assuming the desired separation and pair heading are set at $7R$ and 45° , respectively, and $|M| = 10^4 \text{ A/m}$. One distinction of this new controller is that it lends itself to steer agents in the shortest path along a straight line toward the goal state.

center over a workspace size of 5 cm) located at center of the coil system (see Fig. 9). The strength of magnetic field is smaller than the coercivity of the magnetic materials in the agents, and so the agents magnetization will not be altered by the actuation field. Agent position is detected using a camera (FO134TC, FOculus) mounted atop the workspace, and a computer with custom C++ code finds agent positions using a Hough Circle Transform in the OpenCV library at 60 frames/second. Two identical agents are immersed in a

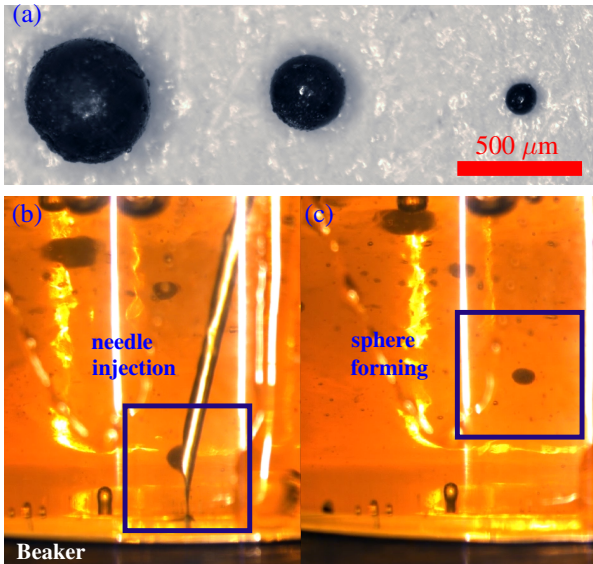


Fig. 8 Spherical microrobots are shown made of (a) Polyurethane combined with magnetic nanoparticles and glass beads. Fluid-assisted fabrication method is illustrated using honey as the fluid with high viscosity inside a Beaker: (b) needle injection followed by needle swirl and capillary force condensation until (c) spheres are formed and cured gradually. A video of the fabrication process is available as supplementary material [S2].

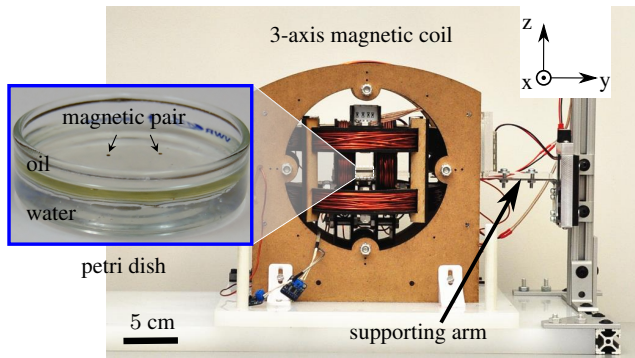


Fig. 9 Experimental setup. In the inset image of agent, two spherical microrobots sit at the interface of water-oil inside a glass petri dish. The identical agents shown have a radius of $250 \mu\text{m}$. The agents are driven in horizontal plane by an electromagnetic coil system with three pairs of coils capable of producing fields in 3D.

glass petri dish and sit at water-oil interface as illustrated in Fig. 9.

4.3 Experiments

Surface tension plays an important role in holding the agents up at the liquid surface. However, capillary force should be treated properly to prevent any pinning effect [22]. This situation happens when the pin at the three-phase contact line (agent-1st liquid-2nd liquid) slips up and down the agent surface; hence it does not allow the spherical agents to roll down across the liquid surface readily. This effect importantly makes it difficult for spheres to rotate out of the plane. To reduce this effect, we chose water-oil interface to decrease the relative surface tension. Moreover, to prevent the agents from sinking, it is required that the

substrate liquid would be denser than the agents. In this respect, we fabricated hollow buoyant spheres using glass beads to hold them up. We tested the introduced controllers for the constrained (one-input) and free 3D magnetization (two-input) modes:

4.3.1 One-input control experiment

Radial and transverse control together: We first test the one-input controller designed for the constrained scenario introduced in 3.1 where the agents' magnetization is constrained to horizontal plane. Fig. 10 shows the experimental results for separation r and pair heading ϕ control (one-input mode) to track a changing goal state. RMS tracking error of less than $47 \mu\text{m}$ and 1.56° is accomplished for the regulation of the separation and the pair heading angle, respectively. It should be noted that there is no tilting angle associated to this single-input controller and agents only rotate in the horizontal motion plane by ψ . However, just to be consistent with the new controller result, α response is shown here too, which is fixed at 90° . Although tracking is achieved, there is a small undesired coupling between the states controllers. Ideally, to be able to independently control r and ϕ , flipping the control angle for transverse control needs to occur instantaneously.

One can confirm by tracking the agent's orientation in the video [S3] in supplementary materials, that the agents remain aligned with the actuation field during the entire experiment. However, the agents take approximately 100 ms to align with the field when it switches direction suddenly. Also, as mentioned earlier, for a rotating actuation field with a constant strength, if the separation between agents becomes too small, not only angle error interference may come to play, but also the appeared local force is hard to overcome by a general controller.

4.3.2 Two-input control experiment

For the two-input control to be effective in practice, we check its underlying assumption that whether the agents always align with the applied field. We ran experiments by applying a rotating field perpendicular to the motion of plane and monitored the rotation of a spherical agent. One can confirm by looking at the video [S3] that the spherical agents rotate with the field smoothly at the water-oil interface and the controller assumption holds. The north pole of the magnetic sphere is marked in green to facilitate this observation.

Fig. 11 shows the experimental results for two-input control to track a changing goal state. RMS tracking error of less than $39 \mu\text{m}$ and 1.45° is accomplished for the regulation of the separation r and the pair heading angle ϕ , respectively. Thus, the two-input controller results in a better performance compared to the transverse and radial force controller, as this controller benefits from the full-actuation system property being able to generate any arbitrary radial and transverse force proportional to error (up to saturation). It can be seen from Fig. 11 that the tilting angle α also varies besides

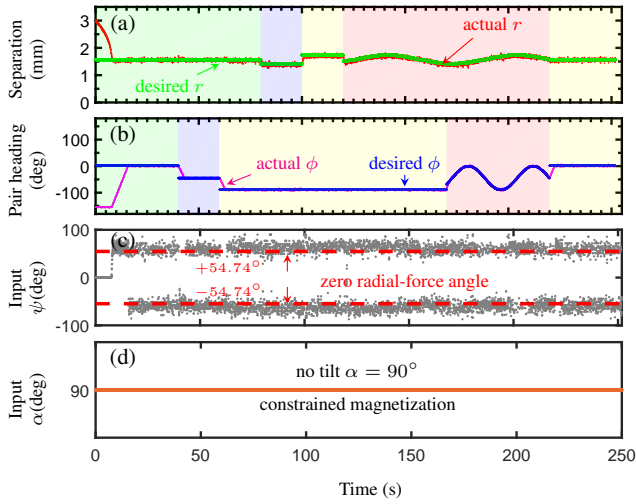


Fig. 10 (a) Separation r and (b) pair heading ϕ tracking using radial and transverse control together at water-oil interface: (c) the in-plane control angle ψ and (d) the out-of-plane tilting control angle α which is fixed at 90° . There is only one control input ψ ; in other words magnetization is constrained to the surface plane and the system is underactuated leading to coupling behavior of the states. RMS tracking error of less than $47 \mu\text{m}$ and 1.56° is accomplished for the regulation of the separation and the pair heading angle, respectively. A video of this experiment is available as supplementary material [S3].

the in-plane angle ψ . The control inputs are bounded and following a trend under the influence of the controller. If there still exists some small error, it might be because of limited feedback rate that causes the agents not to align with the field fast enough. Furthermore, there is only a small improvement in terms of states error observed in the two-input controller with respect to the one-input controller. This observation emphasizes that the one-input control method still works optimally for the constrained mode. For one-input control where the agents' magnetization lies in the horizontal plane, with only ψ input, it is only possible to create either desired radial or transverse forces, and not both. In contrast, in the free 3D magnetization mode where the two-input control appears to be feasible, there are two inputs to control the two state. Hence, they system can be fully actuated.

4.3.3 Center-of-mass control

One can control the center-of-mass (COM) position of the set of agents in addition to the relative states. To this end, a relatively weak 2D magnetic field gradient is superimposed on the uniform field signal. As a result, one can move the agents around to the desired point within the field of view. This idea is demonstrated in video [S3], and the background details to construct the gradient field signal is provided in the supplementary material [S1].

5 Conclusions

In this paper, we explored the 2D motion control of small-scale identical magnetic robots in close proximity with each other. Consistent simulation and experimental

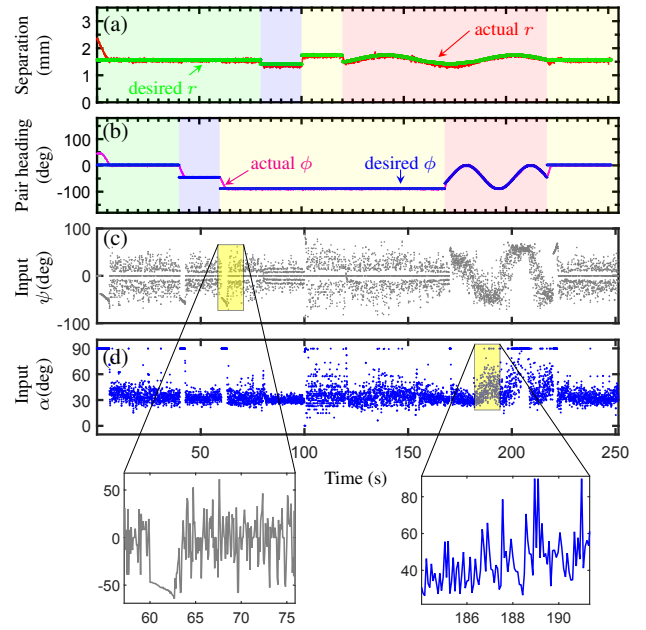


Fig. 11 (a) Separation r and (b) pair heading ϕ tracking using two-input control at water-oil interface: (c) the in-plane control angle ψ and (d) the out-of-plane tilting control angle α . The control angles vary to maintain the desired separation and pair heading states. RMS tracking error of less than $39 \mu\text{m}$ and 1.45° is accomplished for the regulation of the separation and the pair heading angle, respectively. A video of this experiment is available as supplementary material [S3].

results demonstrate that the two-input control method outperforms the one-input control thanks to the feasibility of the out-of-plane rotation. Using the proposed technique any inter-agent separation, heading and position of the set can be maintained via modulation of the inter-agent magnetic forces.

For the controller to operate without instability, the relative spacing between agents in this work needed to be between 2.5 and 30 agents radius. The proposed method is applicable to any magnetic micro/milli-robotic system using hard or soft magnets, either having the coils set up far away or close, and it is possible to be combined with other multi-agent control methods. Control over even smaller separations is practically limited because of the local field overpowers the external field for such small separation distances, agents are susceptible to collision with each other, and existing limit on feedback rate due to higher forces and fast system dynamics. Fluid and capillary interactions were assumed to be negligible in this study. However, it is recommended to analyze these forces for various liquid interfaces.

The proposed principle in this paper has the potential to be scaled up to a larger number of agents for which the system will experience a higher degree of underactuation. To solve this problem a more advanced controller is required. The 2D motion of the immersed agents at the water-oil interface investigated in this paper can be considered as a special case of 3D motion. For 3D motion the number of states will be augmented by one, yet there will be only two input angles available making the system underactuated. Our research will involve dealing with this underactuation property in a similar fashion as we did for 2D motion

with one-input control. Future research will investigate the problem of manipulating multiple agents to complete useful tasks using a team of agents in 3D fluidic environments.

Acknowledgements This work was supported by the Natural Sciences and Engineering Research Council of Canada (NSERC) through the Discovery Grant.

References

- Bradley J Nelson, Ioannis K Kaliakatsos, and Jake J Abbott. Microrobots for minimally invasive medicine. *Annual Review of Biomedical Engineering*, 12:55–85, 2010.
- Edward B Steager, Mahmut Selman Sakar, Ceridwen Magee, Monroe Kennedy, Anthony Cowley, and Vijay Kumar. Automated biomanipulation of single cells using magnetic microrobots. *The International Journal of Robotics Research*, 32(3):346–359, 2013.
- George M Whitesides and Bartosz Grzybowski. Self-assembly at all scales. *Science*, 295(5564):2418–2421, 2002.
- Metin Sitti, Hakan Ceylan, Wenqi Hu, Joshua Giltinan, Mehmet Turan, Sehyuk Yim, and Eric Diller. Biomedical applications of untethered mobile milli/microrobots. *Proceedings of the IEEE*, 103(2):205–224, 2015.
- Eric Diller and Metin Sitti. Three-dimensional programmable assembly by untethered magnetic robotic micro-grippers. *Advanced Functional Materials*, 24(28):4397–4404, 2014.
- Wenqi Hu, Qihui Fan, and Aaron T Ohta. Interactive actuation of multiple opto-thermocapillary flow-addressed bubble microrobots. *Robotics and Biomimetics*, 1(1):1–6, 2014.
- Laurent Arcese, Matthieu Fruchard, and Antoine Ferreira. Adaptive controller and observer for a magnetic microrobot. *IEEE Transactions on Robotics*, 29(4):1060–1067, 2013.
- Jake J Abbott, Marco Cosentino Lagomarsino, Li Zhang, Lixin Dong, and Bradley J Nelson. How should microrobots swim? *The International Journal of Robotics Research*, 28(11-12):1434–1447, 2009.
- Sagar Chowdhury, Wuming Jing, and David J Cappelleri. Controlling multiple microrobots: recent progress and future challenges. *Journal of Micro-Bio Robotics*, 10(1-4):1–11, 2015.
- Eric Diller, Joshua Giltinan, and Metin Sitti. Independent control of multiple magnetic microrobots in three dimensions. *The International Journal of Robotics Research*, 32(5):614–631, 2013.
- J. M. Ng, M. J. Fuerstman, B. A. Grzybowski, H. A. Stone, and G. M. Whitesides. Self-assembly of gears at a fluid/air interface. *Journal of the American Chemical Society*, 125(26):7948–7958, 2003.
- Bartosz A Grzybowski, Howard A Stone, and George M Whitesides. Dynamic self-assembly of magnetized, millimetre-sized objects rotating at a liquid–air interface. *Nature*, 405(6790):1033–1036, 2000.
- Alexey Snezhko and Igor S Aranson. Magnetic manipulation of self-assembled colloidal asters. *Nature Materials*, 10(9):698–703, 2011.
- Sylvain Martel, Mahmood Mohammadi, Ouajdi Felfoul, Zhao Lu, and Pierre Pouponneau. Flagellated magnetotactic bacteria as controlled mri-trackable propulsion and steering systems for medical nanorobots operating in the human microvasculature. *The International Journal of Robotics Research*, 28(4):571–582, 2009.
- David Cappelleri, Dimitrios Efthymiou, Ashesh Goswami, Nikolaos Vitoroulis, and Michael Zavlanos. Towards mobile microrobot swarms for additive micromanufacturing. *International Journal of Advanced Robotic Systems*, 11, 2014.
- Aaron Becker, Yan Ou, Peter Kim, Min Jun Kim, and Agung Julius. Feedback control of many magnetized: Tetrahymena pyriformis cells by exploiting phase inhomogeneity. In *IEEE International Conference on Intelligent Robots and Systems*, pages 3317–3323, 2013.
- Lyes Mellal, David Folio, Karim Belharet, and Antoine Ferreira. Optimal control of multiple magnetic microbeads navigating in microfluidic channels. In *2016 IEEE International Conference on Robotics and Automation (ICRA)*, 2016.
- Eric Diller, Chytra Pawashe, Steven Floyd, and Metin Sitti. Assembly and disassembly of magnetic mobile micro-robots towards deterministic 2-D reconfigurable micro-systems. *The International Journal of Robotics Research*, 30(14):1667–1680, 2011.
- Shuhei Miyashita, Eric Diller, and Metin Sitti. Two-dimensional magnetic micro-module reconfigurations based on inter-modular interactions. *The International Journal of Robotics Research*, 32(5):591–613, 2013.
- Mohammad Salehizadeh and Eric Diller. Two-agent formation control of magnetic microrobots. In *Manipulation, Automation and Robotics at Small Scales (MARSS), International Conference on*, pages 1–6. IEEE, 2016.
- Daniel D Villani, KW Yung, and PB Landecker. An analytic solution for the force between two magnetic dipoles. *Magnetic and electrical Separation*, 9:39–52, 1998.
- Lichao Gao and Thomas J McCarthy. Contact angle hysteresis explained. *Langmuir*, 22(14):6234–6237, 2006.